D 3   Fluid vesicles

In: *Lecture Notes: 'Physics meets Biology. From Soft Matter to Cell Biology'.*

35th Spring School, Institute of Solid State Research, Forschungszentrum Jülich (2004).

U. Seifert

II. Institut für Theoretische Physik

Universität Stuttgart

Contents

1   Introduction

Vesicles constitute a well-defined model system for studying basic physical aspects of the more complex biological cells. These cells consist of a structured inhomogeneous interior, where the nucleus, cell organelles such as ribosomes, mitochondria and the golgi apparatus are embedded in a highly viscous complex fluid formed by all sorts of proteins in an ionic aequous solution. Cells are bounded by the cell membrane, which itself has a complex architecture, sketched in Fig. 1. Its main element is a bilayer of various types of lipids into which proteins such as ion channels and pumps are embedded. The sugar polymers of the outer glycocalix are anchored to this membrane as well as an actin-spectrin network is attached to it on the cellular side in the case of red-blood-cells.
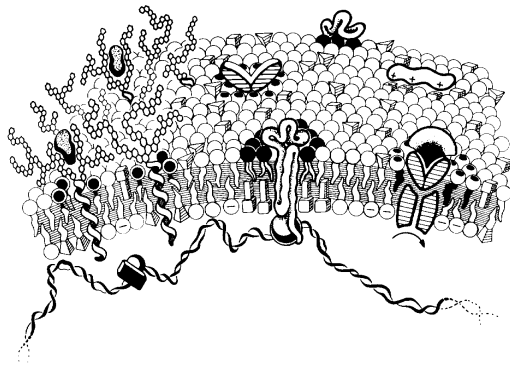

Fig. 1: *Cartoon of the cell membrane*

Vesicles, to the contrary, are formed by a closed lipid bilayer only. Lipid molecules consist of a hydrophilic dipolar or charged head group to which two hydrophobic hydrocarbon chains are attached. In a bilayer these chains are shielded from the aqueous environment. Bilayers form spontaneously in a process of self-aggregation (or self-organization) if lipids are dissolved in aequous solution due to their amphiphilic nature. Given some experience, unilamellar vesicles with sizes of several micron diameter can be obtained. Once a nice vesicle is formed, it can be studied using videomicroscopy, see Fig. 2. Such observations have revealed an amazing variety of shapes, some of which are reminiscent on the shapes of red-blood-cells, despite the fact that vesicles lack so much of the complexity of cells and, in particular, their non-equilibrium nature. A selection of these shapes of various symmetries and topologies is shown in Figs. 3-6.

This variety of shapes among which transformation have been induced by changing the temperature or the osmotic condition prompted in the late eighties an intense and finally successful search for a quantitative physical explanation of these phenomena.

In this lecture, I will outline the basic physical principles of fluid vesicles and their theoretical description focussing on three main topics. In Section 2, the curvature model will be introduced that leads to a quantitative understanding of the whole zoo of vesicle shapes and their thermal fluctuations. Section 3 treats the adhesion or interaction of a vesicle with a substrate. Section 4 deals with the dynamics of vesicles in particular in hydrodynamic flow fields. Such non-equilibrium aspects of vesicles have become increasingly important starting in the mid-nineties.

These lecture notes are mainly pedagogical with only a few selected references. A systematic and comprehensive presentation of the physics of fluid vesicles can be found in the review article [1].
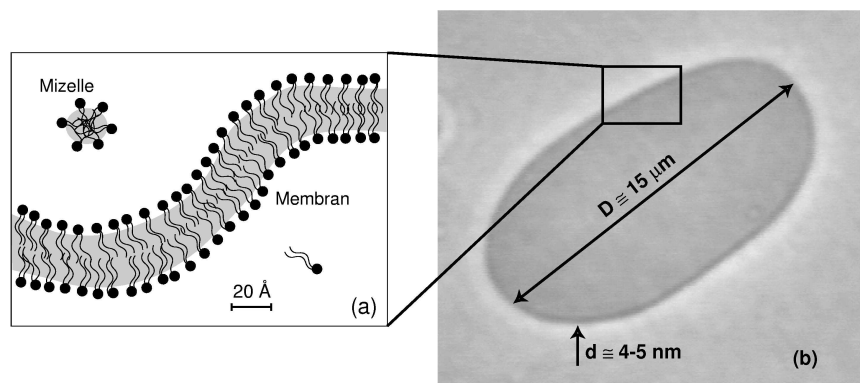
Fig. 2: *Sketch of a lipid bilayer membrane and phase contrast microscopy picture of a giant vesicle (courtesy of H.-G. Döbereiner).*
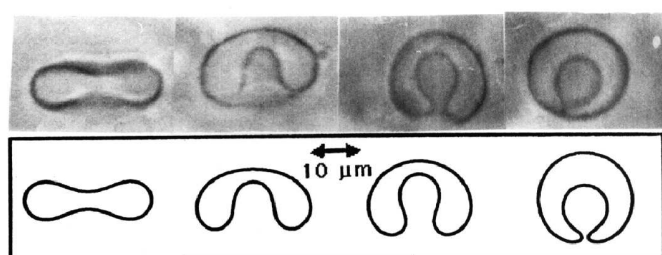

Fig. 3: *Discocyte-stomatocyte transition. With increasing temperature, the up/down symmetric discocyte (left shape) turns into a symmetry-broken stomatocyte. The contours below are calculated based on the bilayer-couple model* [2, 3].

2 Shapes

2.1 Physics of the curvature model

For a physical approach for understanding the factors which determine the variety of vesicle shapes and their transformation we search for an appropriate (free) energy whose minimization yields these shapes. For a symmetric membrane, the chemical composition and environment of both monolayers is identical. Therefore, the flat conformation is locally the state of lowest energy. For a closed configuration, which is necessarily non-flat, the selection of the correct energy has to be guided by the essential physical properties of closed bilayer membranes.

Length-scale separation and curvature model: The bilayer is about 4 nm thick, a giant vesicle is about 10^4 times larger. This separation of length-scales allows to describe the membrane as a two-dimensional surface $\mathbf{R}(s_1, s_2)$ parametrized by two internal coordinates (s_1, s_2) embedded in the three-dimensional space. Any such surface can locally be characterized by the two radii of curvature R_1 and R_2 from which one forms the mean curvature, $H \equiv (1/R_1 + 1/R_2)/2$, and the Gaussian curvature, $K \equiv 1/R_1 R_2$, see Fig. 7. The detailed mathematics is recalled in Appendix A. The basic assumption of the curvature model is that bending such a membrane costs locally the energy [7, 8]

$$f \equiv (\kappa/2)(2H)^2 + \kappa_G K, \tag{1}$$

where κ and κ_G are the ordinary and the Gaussian bending rigidity, respectively. These material parameters have dimension of energy (since f is an energy/area). For phospholipid membranes,
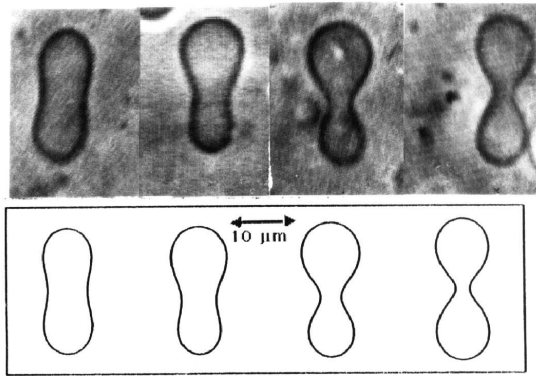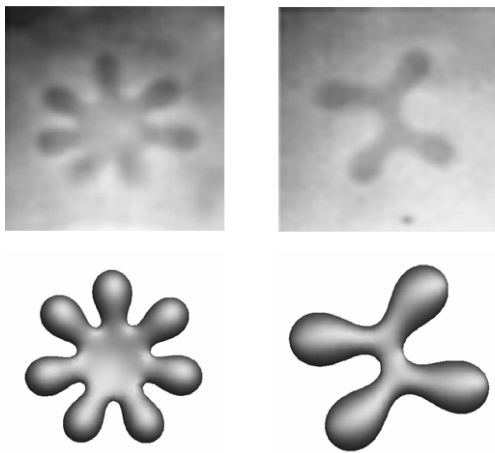
Fig. 4: *Prolate and pear-like shapes* [2, 3].

Fig. 5: *Starfish vesicles as observed experimentally (top) and modelled theoretically (bottom)* [4].

a typical value is 10^{-12} erg $= 10^{-19}$ J.

Large edge energy and fixed topology: Any open edge of a membrane patch exposed to water costs a large energy. This is the reason why free membrane patches do not exist. Likewise, the topology of a vesicle does usually not change since this would imply to form transient edges. Therefore, we have to consider only closed membrane configurations, i.e., vesicles, for which the energy

$$F_\kappa \equiv (\kappa/2) \oint dA(2H)^2 \tag{2}$$

is given by the integral of (1) over its closed surface. Due to the mathematical Gauss-Bonnet theorem the integral of the second term of (1) depends only on the topology (i.e. number of handles g) of a vesicle but not on its shape, i.e. $\oint K dA = 4\pi(1 - g)$. Therefore, this second term can be discarded as long as we consider vesicles of fixed topology.

Fluidity, insolubility and incompressibility: Since the membrane is in the fluid state of matter, it cannot withstand shear in its plane. Moreover, the solubility of the double chain phospholipids is extremely low. Therefore, there is practically no exchange of material between membrane and solution. This fact together with the quite small compressibility of the membrane implies that for almost all vesicle phenomena the membrane can be considered as locally incompressible. For a closed vesicle, the total area A is thus fixed.
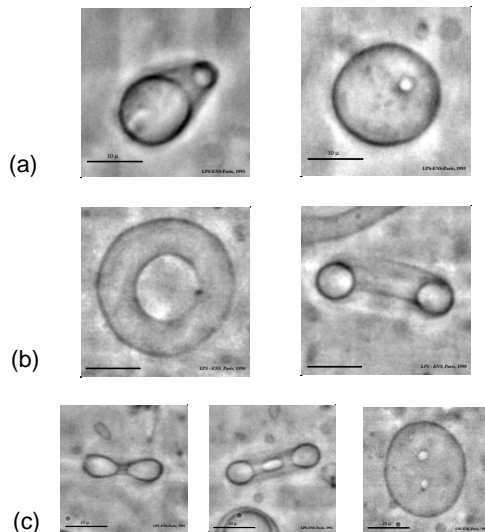
Fig. 6: *Shapes of non-spherical topology. a) a non-axisymmetric torus, b) an axi-symmetric circular torus, c) the "button" surface of genus 2* [5, 6].
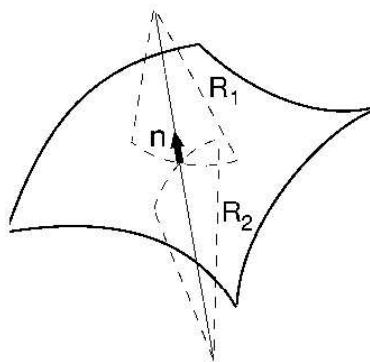

Fig. 7: *Local radii of curvature R_1 and R_2 and normal vector $\mathbf{n}$ of a membrane patch.*

Osmotic control of volume: Experimentally, one controls in these systems often the osmotic conditions of the external solution. Even if one works with "pure water", there are necessarily osmotically active impurities around. Since the membrane is permeable for water, the volume changes up the point where practically no more osmotic pressure difference acts. The bending moments that can be derived from (2) are just too weak to balance any non-zero osmotic pressure. Therefore, vesicle configurations must be determined at a prescribed volume V.

2.2   Phase diagram of a minimal model

We are now looking for the shapes which minimize the curvature energy (2) for given area A and volume V. These constraints are added with Lagrange multipliers Σ and P to the energy (2) which leads to

$$F \equiv F_\kappa + \Sigma A + PV. \tag{3}$$

The minimization of (3) must be performed numerically. This is done by solving the Euler-Lagrange-equations, $\delta^1 F = 0$, in a suitable parametrization of an axisymmetric shape [9]. This procedure leads to stationary shapes which are local minima and saddle points in the shape

space, among which careful inspection of the energy diagrams allows to distinguish. The stationary shapes depend only on one parameter which is the reduced volume

$$v \equiv V/[(4\pi/3)(A/4\pi)^{3/2}]. \tag{4}$$

The value of the bending rigidity κ will not affect the result at this stage, since κ is the only energy scale in the problem.

It turns out that there are three types or "branches" of local minima: prolates/dumbbells, oblates/discocytes and cup-shaped stomatocytes, see Figs. 8,9. Obviously, this minimal model captures important aspects of vesicle shapes since we obtain theoretically shapes found previously in the lab. However, something important is missing since this minimization does not lead to pear-like shapes as shown in Fig. 4 or starfish vesicles as shown in Fig. 5. The very observation of these shapes proves that the model described so far is incomplete.
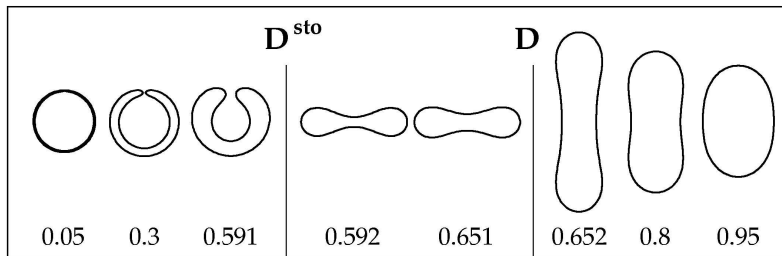
Fig. 8: *Shapes of minimal curvature energy F_κ for various values of the reduced volume v. The shapes of lowest energy are prolate for $v \gtrsim 0.65$, oblate for $0.65 \gtrsim v \gtrsim 0.59$, and stomatocyte for $v \lesssim 0.59$ [9].*
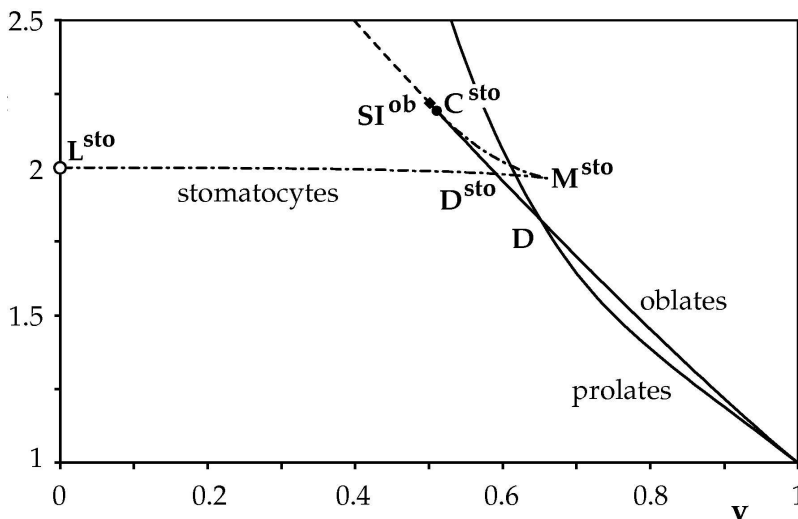
Fig. 9: *Curvature energy $F_\kappa/8\pi\kappa$ of the stationary shapes $[\delta^1 F = 0]$ as a function of the reduced volume v. D and D^{sto} denote the two discontinuous transitions shown in Fig. 8. The further capital letters denote distinct points described in detail in* [9].

2.3   Refined curvature models

The missing ingredient in (2) is the fact that it is not possible to describe the membrane just as a structure-less two dimensional surface. One key signature of its molecular architecture must be retained and that is the bilayer feature [10, 11]. The two monolayers are tightly coupled but the exchange of lipid molecules between them is slow compared to the experimental time-scale of these observations. Therefore, the numbers N^+ and N^- of molecules in the outer and inner monolayer, respectively, are conserved. The number difference $N^+ - N^-$ leads to a prefered area-difference

$$\Delta A_0 \equiv (N^+ - N^-)a_0 \tag{5}$$

between the two layers. Here, a_0 is the equilibrium area per lipid molecule. The actual area difference, $\Delta A = A^+ - A^-$, can be expressed as an integral over the mean curvature as

$$\Delta A = 2D \oint dA \, H \tag{6}$$

where D is the distance between the neutral surfaces of the two monolayers, i.e., roughly half the bilayer thickness. If the area of each molecule was strictly conserved, ΔA would be conserved too. This would lead to a third constraint on the total mean curvature

$$M \equiv \oint H dA. \tag{7}$$

Such a model had become popular under the name of the bilayer couple model [11, 2]. Detailed comparisons with experiments and a thorough theoretical analysis of bilayer bending finally revealed that this hard constraint on ΔA must be softened [12]. The correct form of the bilayer feature is therefore to add to F_κ an area difference elasticity,

$$F_{ADE} = \frac{\alpha \pi \kappa}{2D^2 A}(\Delta A - \Delta A_0)^2, \tag{8}$$

where α is somewhat model dependent but close to 1.
Minimizing the total energy,

$$F \equiv F_\kappa + F_{ADE} , \tag{9}$$

now leads indeed to pears, shapes and a multitude of starfish vesicles [12, 13, 4]. In this model, the minimal shapes depend not just on the reduced volume v but on one more parameter

$$\bar{m}_0 \equiv \Delta A_0/2DR, \tag{10}$$

which is basically a scaled "frozen-in" number difference of lipid molecules in the two layers. The shapes of lowest energy can be arranged in a two-dimensional phase diagram [12, 13], see Fig. 10. As one changes temperature or the osmotic conditions, the parameters v and $\bar{m}_0$ change due to thermal expansion of the area [9]. Thus, a trajectory in this phase diagram cuts across the different region of stability of the different shapes. Transitions from one shape to another, say from prolate to pear, can be abrupt (i.e., discontinuous, or first order) or smooth (i.e. continuous or second order). All experiments performed so far on the shapes of such vesicles and their transitions seem to be quantitatively compatible with this theoretical model.
The discussion so far has been confined to membranes which are symmetric with respect to both the chemical composition of the two leaflets of the bilayer and the liquid environment.
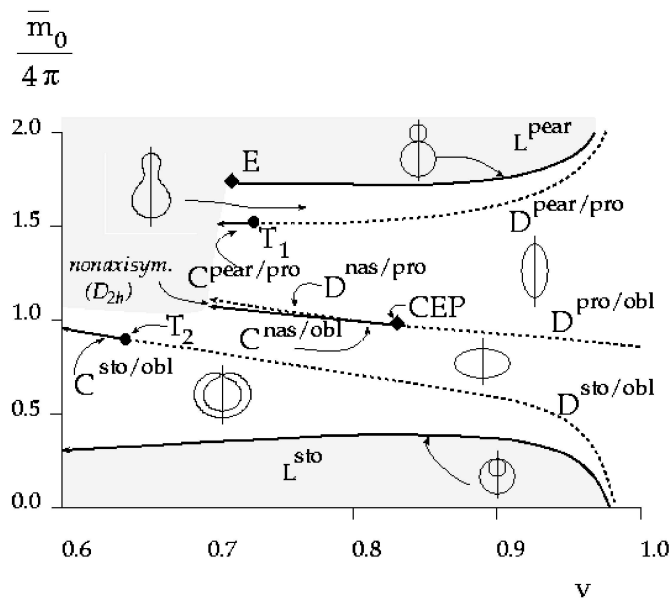
Fig. 10: *Phase diagram of the ADE model. Shown are the shapes of lowest energy as a function of the reduced volume v and the scaled prefered area-difference $\bar{m}_0$ for $\alpha = 1.4$. The capital letters denote shape transitions, limiting lines and special points. The region of stable starfish vesicles lies at smaller v [13] .*

Originally, Helfrich suggested a spontaneous curvature model in which $(2H)$ in (2) is replaced by $(2H - C_0)$ [8, 14]. In this case, C_0 is the curvature that a free membrane patch cut from a vesicle in a Gedanken-experiment would acquire spontaneously. One can show that minimizing such a modified energy (2) leads to the same multitude of shapes as minimizing (9) although with different stability properties [12, 15]. Even for a vesicle under such asymmetric conditions the second energy term in (9) must be retained if its two leaflets do not exchange molecules. In the latter case, the spontaneous curvature and the area difference term can then be combined into an "effective" spontaneous curvature.

Minimization of the curvature energy happens at fixed topology, so far spherical topology. For vesicles of higher topology as those shown in Fig. 6, similar phase diagrams have been calculated [16, 17]. For surfaces with genus $g \geq 2$ an interesting new phenomenon occurs. The fact that F_κ in (2) is invariant under conformal transformation of the three-dimensional space, leads to a continuous degeneracy of the shape of minimal energy at fixed v and $\bar{m}_0$. This phenomenon, called conformal diffusion, has been first predicted theoretically [17] and later been verified experimentally [4].

2.4   Thermal fluctuations

The vesicle shapes obtained by minimizing the appropriate curvature energy subject to the geometric constraints formally correspond to solving a zero temperature problem. Video microscopy reveals that these shapes typically exhibit visible thermal fluctuations [18]. How can

these fluctuations be described?

It is instructive to start from a planar membrane. The local position of such a membrane with respect to the mean plane can be parametrized by a height variable $h(x, y)$. The energy (2) then becomes

$$F_\kappa = \frac{\kappa}{2} \int dx dy (\nabla^2 h)^2 = \frac{\kappa}{2} \int \frac{d^2 q}{(2\pi)^2} q^4 h_{\mathbf{q}} h_{\mathbf{q}}^* \tag{11}$$

where the Fourier transformation is defined as

$$h(\mathbf{x}) \equiv \int \frac{d^2 q}{(2\pi)^2} h_{\mathbf{q}} e^{i\mathbf{q}\mathbf{x}} . \tag{12}$$

Invoking the equipartition theorem [19] then tells us the mean amplitudes at temperature T

$$< |h_{\mathbf{q}}|^2 > = \frac{k_B T}{\kappa q^4}, \tag{13}$$

where $< ... >$ is the thermal expectation value taken with the Boltzmann weight, $\exp(-F_\kappa/k_B T)$. In principle, one could attempt to calculate the fluctuations around any of the zero temperature $(T = 0)$ shapes using a similar approach. In practice, the differential geometry involved is tricky and taking care of the geometrical constraints is not entirely trivial. The latter problem can be solved by introducing an effective tension and pressure difference whose numerical value are given by the Lagrange multiplier Σ and P, used to implement the area and volume constraints, respectively [15]. The former must be attacked numerically which is somewhat cumbersome. So far, only a few attempts have been made to calculate such fluctuation spectra around non-trivial $(T = 0)$ shapes [20, 21, 22]. The notable exception are quasi-spherical vesicles from whose fluctuation spectrum the value of the bending rigidity can be deduced by comparing data to theory, for relatively recent work, see e.g. [23, 24].

In a very recent development, fluctuation around non-spherical shapes can be simulated numerically and then be compared to experimental spectra. This technique allows a precise determination of membrane parameters like bending rigidity and spontaneous curvature [25].

3 Adhesion

3.1 Two length scales

From the point of view of having a well-defined system, an isolated vesicle freely floating in solution is almost perfect. For interesting applications or a higher level in complexity, interaction of the vesicle with other objects should be considered. The conceptually simplest case corresponds to adhesion of a vesicle to a rigid substrate. For this case, a comprehensive set of experimental data can be obtained using reflection interference microscopy [26, 27]. This technique allows not only to study the gross features of a bound vesicle such as its contour radius or the size of the adhesion disc but also the fluctuation spectrum of its bound part. Such experiments show clearly that the problem of a vesicle adhering to a substrate has two complementary aspects, a macroscopic one (overall shape) and a mesoscopic one (fluctuation spectrum in the vicinity of the substrate), see Fig. 11. Recognizing in a first step this distinction, is key for a successful theoretical modeling of this problem. In a second step, the two aspects must be reconciled self-consistently.
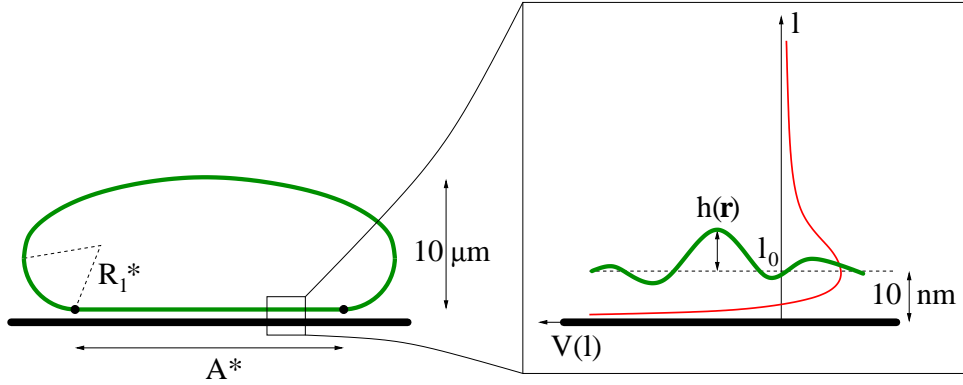
Fig. 11: *Adhesion of vesicles: Macroscopic view with contact area A^* and contact curvature $1/R_1^*$ and mesoscopic view with the bound part fluctuating in a potential $V(l)$ which has a minimum typically $\simeq 10$ nm above the substrate.*

3.2 Macroscopic model

From the macroscopic perspective, a minimal model for adhesion of a vesicle to a substrate consists in adding an adhesion energy

$$F_a \equiv -W A^* \tag{14}$$

to the bending energy (2) [28]. Here, W is the contact potential and A^* the size of the adhesion patch with which the vesicle adheres to the substrate. Such a contact potential enters the boundary condition at the point of contact. First, the contact angle is necessarily π since any sharp bend would have an infinite curvature energy. This implies that the membrane is curved only in one direction and $1/R_2^* = 0$ along the line of contact. Second, the contact curvature obeys

$$1/R_1^* = (2W/\kappa)^{1/2} , \tag{15}$$

which follows from minimizing with respect to the area of contact [28]. This boundary condition, which does not depend on the area of the vesicle, holds for all variants of the curvature model. Depending on both the size of the vesicle,

$$R \equiv (A/4\pi)^{1/2} , \tag{16}$$

and the strength of the adhesion potential W, adhesion can either be "weak" or "strong". The crucial quantity is the scaled strength of the adhesion potential

$$w \equiv W R^2/\kappa . \tag{17}$$

Typical bound shapes as those shown in Fig. 12 demonstrate that there are two regimes.

Weak adhesion (w of order 1): It turns out, somewhat surprisingly, that one needs a threshold value w_c for adhesion to occur. If the adhesion strength is too small, the possible gain in adhesion energy is smaller that the cost in deforming its shape so that the vesicle will not adhere even in the presence of the weakly attractive substrate [28]. The specific value of w_c depends on the reduced volume but is of order 1, see Fig. 13 [29]. For $w > w_c$, the vesicle is bound. Its contact area A^* increases with increasing strength of the potential W.
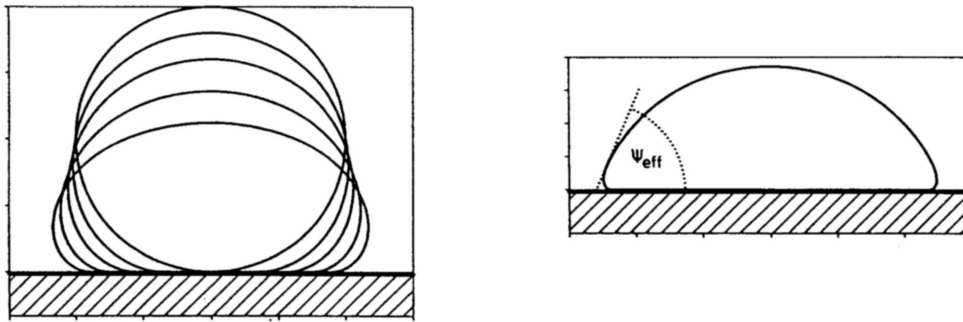
Fig. 12: *Calculated shapes of bound vesicles. (Left): regime of weak adhesion; (right): regime of strong adhesion. The latter shape is almost spherical cap-like with an effective contact angle Ψ_{eff} [28].*

Strong adhesion ($w >> 1$): Physically, in this regime, the bending energy becomes irrelevant and the shape is determined solely by the desire to maximize the contact area A^* for given total area and enclosed volume. The optimal shape then is a spherical cap with an effective contact angle $\Psi_{\mathrm{eff}}(v)$ determined by the geometrical constraints, see Fig. 12. The explicit relation $\Psi_{\mathrm{eff}}(v)$ is given in [30]. The limiting cases are $\Psi_{\mathrm{eff}} = \pi$ for a sphere ($v = 1$) and $\Psi_{\mathrm{eff}} = 0$ for a flat pancake ($v = 0$). Interestingly, this effective contact angle also obeys a Young equation [28],

$$W = \Sigma(1 + \cos \Psi_{\mathrm{eff}}). \tag{18}$$

In contrast to adhesion of liquid droplets where Σ would be the surface tension, for vesicle adhesion Σ is not an independent quantity but rather given by the (numerical) value of the Lagrange multiplier used to implement the area constraint. As (18) shows, Σ is a function of both the reduced volume (through $\Psi_{\mathrm{eff}}(v)$) and of the adhesion strength W.
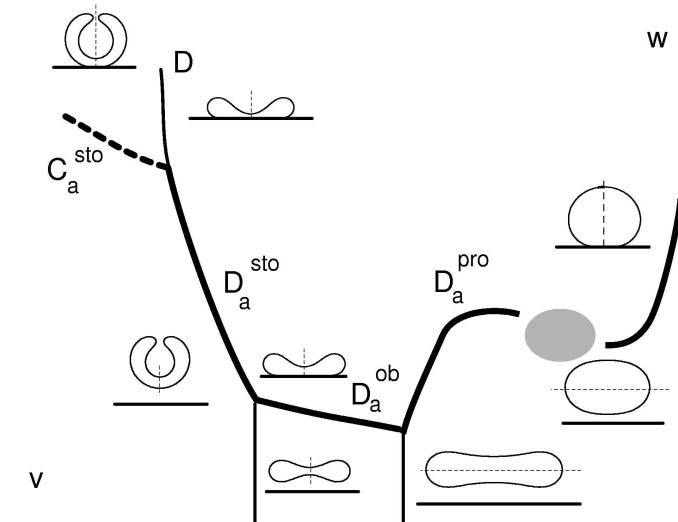

Fig. 13: *Semiquantitative phase diagram for adhering vesicles as a function of adhesion energy w and reduced volume v. The thick lines denote the curvature driven adhesion transition $w_c(v)$. Depending on the reduced volume v, bound and free shapes can be prolate, oblate or stomatocyte-like [29].*

Experimentally, the difference between strong and weak adhesion has clearly been seen. With light microscopy [31], the mutual interaction of vesicles has been studied and large rounded contact regions corresponding to weak adhesion were found. Spherical cap-like configurations have been seen in micro-pipet experiments [32] as well as in freeze-fracture electron microscopy for smaller vesicles [33].

From the macroscopic point of view, the problem of a vesicle adhering to a substrate is thus solved if we know the strength of the contact potential W which must be extracted from a more mesoscopic approach.

3.3 Mesoscopic description

The bound part of a closed vesicle is typically several nanometers away from the substrate and still shows thermal fluctuations [27]. These conditions require that we refine our modeling by paying due attention to the mesoscopic interactions between membrane and substrate. As reviewed in [34], various forces are involved in this interaction such as van der Waals interaction, electrostatic contributions in the case of charged membranes, and short range repulsive forces such as the hydration force or protrusion forces. All these direct forces can be combined into an effective potential $V_d(l)$. This quantity gives the energy of a (fluctuationless) planar membrane at a distance l from the substrate. Typically $V_d(l)$ increases dramatically for small l and vanishes for large l. In between, there are either one or two minima. If these direct forces were the full story, we could take as the effective adhesion strength of the macroscopic approach the value of the direct potential at the minimum l_0, i.e. $W = -V_d(l_0)$. However, the situation is more complex due to thermal fluctuations.

The presence of the substrate confines its fluctuations [35]. As derived in Appendix B, this effect can be described by a steric or fluctuation potential [30]

$$V_f(\Sigma; l) = \left(\frac{6b^2(k_B T)^2}{\kappa l^2} \right) \left(\frac{y^2}{\sinh^2 y} \right) \ \text{ with } \ y \equiv (\Sigma/bT)^{1/2} l/2 \ \text{ and } \ b \simeq 1/2\pi. \quad (19)$$

This potential expresses the increase in free energy due to a decreasing entropy for thermal fluctuations with increasing confinement. It diverges as $1/l^2$ for $l \to 0$ and vanishes for $l \to \infty$.

Within a superposition approach, the fluctuation potential $V_f(\Sigma; l)$ should be added to the direct potential $V_d(l)$ to form the total potential $V(l) \equiv V_d(l) + V_f(\Sigma; l)$. The energy of the bound part of the vesicle, which is at a local distance $l(x, y)$ from the substrate, is then given by

$$F_a = \int dA \left\{ \frac{\kappa}{2} (\nabla^2 l)^2 + V(l) + \Sigma \right\} \approx \frac{1}{2} \int \frac{d^2 q}{(2\pi)^2} \left(\kappa q^4 + (\Sigma - W) q^2 + V''(l_0) \right) |h_{\mathbf{q}}|^2. \quad (20)$$

In the first equality we have to include Σ from the area constraint. The second equality follows after expanding for small fluctuations,

$$h(x, y) \equiv l(x, y) - l_0, \quad (21)$$

around the minimum at l_0. The area element dA becomes

$$dA \approx dx\, dy (1 + (\nabla h)^2/2) \quad (22)$$

and for the potential $V(l)$ an expansion reads

$$V(l) \approx -W + V''(l_0)h^2/2. \tag{23}$$

The prefactor of the q^2 term in (20) is the effective tension

$$\bar{\Sigma} \equiv (\Sigma - W) = -W \frac{\cos \Psi_{\text{eff}}}{1 + \cos \Psi_{\text{eff}}}, \tag{24}$$

which carries two contributions. The first arises from the area constraint, which acts like an external pulling force at the bound part of the membrane. The second one describes the fact that a fluctuating membrane exposes more area to the attractive potential minimum [36]. The final equality, which arises from using (18), shows that for strong adhesion there is a universal relation between the effective adhesion energy W and the effective tension $\bar{\Sigma}$ acting on the fluctuations of the bound part. This relation depends only on the reduced volume v which determines Ψ_{eff}. This relation states in particular that the effective tension becomes negative for those vesicles with a relatively small reduced volume for which $\Psi_{\text{eff}} < \pi/2$. Such a negative tension should show up in the measurable spectrum of fluctuations of the bound part [27], which can be obtained using equipartition on (20) as

$$< |h_{\mathbf{q}}|^2 > = \frac{k_B T}{\kappa q^4 + \bar{\Sigma} q^2 + V''(l_0)}. \tag{25}$$

The final step in a self-consistent description consists in determining not only the ratio between the tension Σ and the depth of the adhesion potential W as given by (24) but also their individual value. Since W corresponds to the depth of the total potential at its minimum l_0, one has

$$W = -[V_d(l_0) + V_f(\Sigma; l_0)]. \tag{26}$$

With this equation, the problem of vesicle adhesion taking into account steric repulsion is closed and solvable for any given form of the direct potential $V_d(l)$. For a specific example, see [30], where the distinction between Σ and $\bar{\Sigma}$ was not yet made. This refinement is irrelevant for large reduced volume or tense vesicles which were the focus in [30] but becomes important for small reduced volume where this refinement [36] predicts a negative $\bar{\Sigma}$.

3.4   Unbinding transition

Two mechanisms for an adhesion or unbinding transition for vesicles should be distinguished. Ignoring fluctuations, the competition between adhesion energy and bending energy predicts a scale dependent adhesion transition at $w_c(v)$. For given W, this relation implies that large vesicles with $R > R_c \equiv (w_c \kappa / W)^{1/2}$ are predicted to adhere while smaller ones are free [28]. Physically, the large ones can take advantage of the adhesion energy without having to pay too much in bending.

The second mechanism happens via fluctuations. Even if the direct potential V_d has a minimum at l_0 with $V_d(l_0) < 0$, thermal fluctuations can be so strong that the membrane prefers to be unbound. This unbinding transition has been studied first for free planar tensionless membranes [37, 38]. The theory described above shows that a similar effect also holds for the vesicles except for quite tense ones [30]. In the latter case the fluctuations may be restricted so much that such a vesicle is still bound even though an open membrane patch (with $\Sigma = 0$) would

unbind due to fluctuations. This regime corresponds to genuine tension-induced adhesion [39]. The crossover between the two different mechanisms can be estimated to happen at a length-scale in the 100 nm range [28].

3.5 Gravity

A particular type of adhesion arises from gravitational effects often used in the laboratory to stabilize vesicles at the bottom of a measuring chamber. If a vesicle is filled with a fluid slightly denser than the surrounding aqueous solution, it will sink to the substrate. Even without an explicit adhesion energy, this geometrical confinement leads to shape changes [40]. The phase diagram is shown in Fig. 14 as a function of the reduced volume v and the (dimensionless) gravitational interaction

$$g \equiv g_0 \Delta \rho R^4 / \kappa, \qquad (27)$$

where $g_0 \simeq 9.81$ m/s^2 and $\Delta \rho$ is the density difference between the aqueous solutions inside and outside the vesicle.
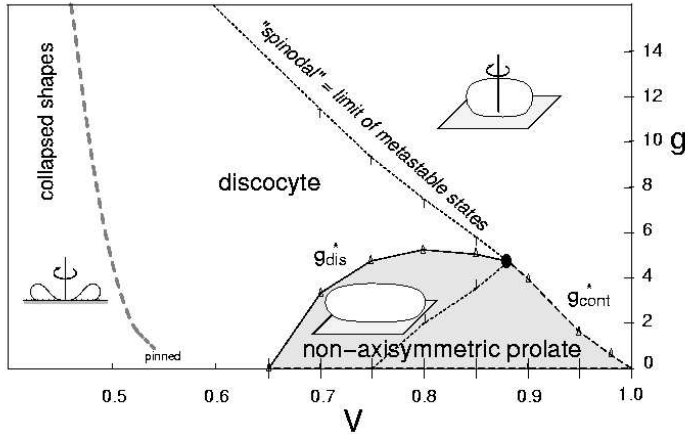

Fig. 14: *Phase diagram including gravity as a function of reduced volume v and gravitational parameter g. In the grey area, the minimal shape is a non-axisymmetric prolate, for larger g an axisymmetric oblate. The transition between the prolate and the oblate is continuous along g_{cont}^* and discontinuous (with associated spinodal) along g_{dis} [40].*

4 Dynamics

4.1 Classification and dissipative mechanisms

Characteristic for giant vesicles is their slow dynamics visible in the microscope. The typical time-scale for shape changes on the micron scale lies in the range of a second which makes vesicles a perfect system to study dynamical aspects in real space directly. For a classification of vesicle dynamics, one has to distinguish dynamics in equilibrium from non-equilibrium phenomena.
Equilibrium dynamics of vesicles comprises the dynamical fluctuations around locally stable mean shapes. *Non-equilibrium dynamics* is the more challenging and less well explored regime. One should distinguish two classes. First, there is relaxation into a new equilibrium after a

parameter change. This class comprises the decay of a metastable shape such, e.g., as the budding process induced by raising the temperature [3, 41]. The driving force in this case is the curvature energy which favors a different shape at the new external conditions. Conceptually related is the spectacular pearling instability of cylindrical vesicles, which develops upon action of optical tweezers [42]. In this case, the laser generates a tension for which a homogeneous cylinder is no longer a stable configuration. The second class of nonequilibrium behavior refers to genuine non-equilibrium states of vesicles induced by external fields such as hydrodynamic flow as described below.

Dynamics in the micron world of vesicles is overdamped, i.e. inertial effects can safely be ignored [43]. This realm is often somewhat counter-intuitive to our experience of fluid phenomena shaped mostly by the so-called large Reynolds number regime where inertia matters. For example, in the micron world, motion is reversible and objects come to rest right after the driving forces cease to act. Driving forces for vesicles arise from bending energy and from external fields such as optical tweezers or hydrodynamic flow. Dissipation (or "friction") takes place both in the surrounding liquid and in the membrane, in principle. For giant vesicles of micron size, the dominant dissipation is viscous dissipation in the embedding fluid [44], which requires a full treatment of the hydrodynamics of this fluid.

Dissipation in the membrane can be classified into three phenomena: Drag between the two monolayers [45], shear viscosity within each layer and permeation through the membrane. Calculation of the relaxation spectra of bending fluctuations involving the first two mechanisms show that on scales of microns and larger, hydrodynamic dissipation is dominant [46]. In the submicron range, friction between the layers becomes relevant. On even smaller scales of several tenths of nanometers, shear viscosity within each layer should be included. Finally, permeation through the membrane seems to be irrelevant on all length-scales with the possible exception of membranes in the vicinity of a substrate [47]. Based on this hierarchy of dissipative mechanisms, for giant vesicles it is often permissible to ignore all but viscous dissipation in the surrounding liquid, as we will do in the following.

4.2   Equation of motion

We now derive the equation of motion for a fluid membrane embedded in a viscous liquid [48]. From a conceptual point of view, it is best to start with the Navier-Stokes equation for the surrounding incompressible liquid given by

$$\rho(\partial_t \mathbf{v} + \mathbf{v}\nabla v) = -\nabla p + \eta\nabla^2\mathbf{v} + \mathbf{f}(\mathbf{r}) \tag{28}$$

$$\nabla\mathbf{v} = 0 \tag{29}$$

where $\mathbf{v}(\mathbf{r})$ is the 3-d velocity field of the liquid with density ρ. $p(\mathbf{r})$ is the local pressure which is basically determined by the incompressibility condition (29). η is the shear viscosity of the liquid (with $\eta \simeq 10^{-3}$ Js/m^3 for water at room temperature), and $\mathbf{f}(\mathbf{r})$ is the force density acting on the liquid. Fortunately, we don't have to deal with the full non-linear Navier-Stokes equation because the left-hand side (lhs) of equation (28), the inertia and connective terms, is much smaller than the right-hand side (rhs) for typical membrane dynamics. This can be understood by defining the Reynolds number

$$Re \equiv \left(\frac{\rho v_{\text{typ}}}{T_{\text{typ}}}\right) / \left(\frac{\eta v_{\text{typ}}}{L_{\text{typ}}^2}\right) = \frac{\rho L_{\text{typ}}^2}{\eta T_{\text{typ}}} \tag{30}$$

as the ratio between the lhs and the rhs. Here, v_{typ}, L_{typ} and T_{typ} are typical velocities, length-scales and time-scales. Choosing $\rho = 10^3 \text{ Js}^2 / \text{ m}^4$, $L_{\text{typ}} = 1\mu\text{m}$, $\eta = 10^{-3} \text{ Js/m}^3$ we get $Re = 10^{-6}$ for $T_{\text{typ}} = 1$ s and $Re = 10^{-3}$ for $T_{\text{typ}} = 10^{-3}$s. So on time-scales accessible to video-microscopy, the Reynolds number Re is small and the lhs of (28) can be neglected. This defines the regime of Stokes-flow governed by

$$\nabla p - \eta \nabla^2 \mathbf{v} = \mathbf{f}(\mathbf{r})$$
$$\nabla \mathbf{v} = 0. \tag{31}$$

The general solution of these inhomogeneous linear equations is given by the super-position of a solution of the homogeneous equation, $\mathbf{v}^{\text{ex}}(\mathbf{r})$, which is typically the externally imposed flow field, and a special solution

$$\mathbf{v}^{\text{ind}}(\mathbf{r}) = \int d\mathbf{r}' \mathcal{O}(\mathbf{r}, \mathbf{r}') \mathbf{f}(\mathbf{r}'), \tag{32}$$

of the inhomogeneous equation. The Green's function for (31) is called the Oseen-tensor $\mathcal{O}(\mathbf{r}, \mathbf{r}')$. As shown in Appendix C, for infinite flow, the Oseen tensor $\mathcal{O}(\mathbf{r}, \mathbf{r}')$ has Cartesian matrix elements

$$\mathcal{O}_{\alpha\beta}(\mathbf{r}, \mathbf{r}') \equiv \frac{1}{8\pi\eta|\mathbf{r} - \mathbf{r}'|} \left[\delta_{\alpha\beta} + \frac{(r_\alpha - r'_\alpha)(r_\beta - r'_\beta)}{|\mathbf{r} - \mathbf{r}'|^2} \right]. \tag{33}$$

Thus, the hydrodynamics mediates a long-range interaction ($\sim 1/|\mathbf{r} - \mathbf{r}'|$) between the force $\mathbf{f}$ acting at $\mathbf{r}'$ and the velocity $\mathbf{v}$ induced at $\mathbf{r}$. The total velocity field becomes

$$\mathbf{v}(\mathbf{r}) = \mathbf{v}^{\text{ex}}(\mathbf{r}) + \mathbf{v}^{\text{ind}}(\mathbf{r}). \tag{34}$$

Such a simple superposition is possible since the Stokes equation is linear due to the absence of the convective term.
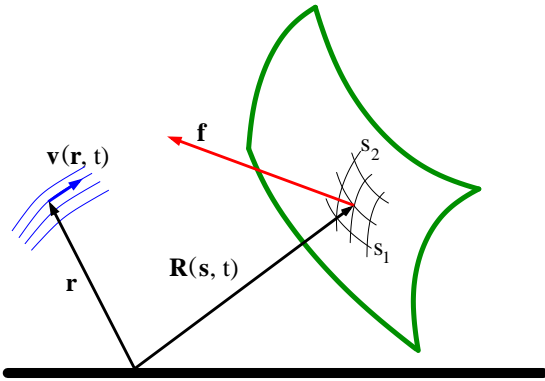
Fig. 15: *Sketch of the hydrodynamic set-up: The membrane at $\mathbf{r}' = \mathbf{R}(s_1, s_2, t)$ exerts a force $f(\mathbf{r}')$ onto the liquid which affects the velocity $\mathbf{v}(\mathbf{r})$.*

The force density $\mathbf{f}(\mathbf{r}')$ arises from both the embedded membrane and from boundary conditions at confining surfaces, see Fig. 15. If the membrane is locally in a non-equilibrium configuration, it wants to change its shape accordingly which acts as a force on the liquid. The formal

expression of this effect is

$$\mathbf{f}(\mathbf{r}') \equiv -\int ds_1 ds_2 \sqrt{g} \left(\frac{1}{\sqrt{g}} \frac{\delta F}{\delta \mathbf{R}} \right) \delta(\mathbf{r}' - \mathbf{R}(s_1, s_2)). \tag{35}$$

This 3-d force density is localized along the two-dimensional membrane as expressed by the δ-function and the integration over the membrane surface. The driving force arises from the variational derivative (virtual displacement) of the appropriate energy F. In a minimal model

$$F = F_\kappa + F_\Sigma, \tag{36}$$

where F_κ is the curvature energy (2). The second term

$$F_\Sigma \equiv \oint dA \, \Sigma(s_1, s_2) \tag{37}$$

is necessary in the dynamics to ensure local area conservation as discussed below. Explicitly, the force density then reads

$$\left(\frac{1}{\sqrt{g}} \frac{\delta F}{\delta \mathbf{R}} \right) = \left(-2\Sigma H + \kappa[(2H)(2H^2 - 2K) + 2\Delta H] \right) \mathbf{n} - g^{ij} \mathbf{R}_i \partial_j \Sigma. \tag{38}$$

Here,

$$\Delta \equiv (1/\sqrt{g}) \partial_i (g^{ij} \sqrt{g} \partial_j) = g^{ij} \partial_i \partial_j. \tag{39}$$

is the Laplace–Beltrami operator on the surface. The normal part of (38) [49] corresponds to the stationarity condition $[\delta^1 F_\kappa = 0]$ discussed in Section 2. The tangential part arises from inhomogeneities in the surface tension $\Sigma(s_1, s_2)$ which will be needed to ensure local incompressibility of the induced flow.

For given forces $\mathbf{f}(\mathbf{r}')$ we know through (32) and (33) the velocity field $\mathbf{v}(\mathbf{r})$ anywhere in the liquid. Hence, we know $\mathbf{v}(\mathbf{r})$ particularly at the location of the membrane $\mathbf{R}(s_1, s_2; t)$ (where we make the time-dependence of the configuration explicit). Since the membrane is impermeable to water flow, the normal velocity of the fluid at the membrane pushes along the membrane and leads to a shape change. Tangential motion of the fluid along the membrane induces lipid flow within the membrane. As boundary conditions for this tangential flow one uses so-called non-slip boundary conditions for which the tangential velocity of the liquid and the induced lipid flow in the membrane are equal. Therefore, the velocity field leads to an equation of motion for the membrane as

$$\partial_t \mathbf{R}(s_1, s_2, t) = \mathbf{v}(\mathbf{R}(s_1, s_2, t)) = v^{\text{ex}}(\mathbf{R}(s_1, s_2, t)) + \mathbf{v}^{\text{ind}}(\mathbf{R}(s_1, s_2, t)). \tag{40}$$

This deterministic equation of motion includes both, normal motion that signifies a shape change of the membrane, and tangential motion that corresponds to lipid flow within the membrane. The so far unknown local tension $\Sigma(s_1, s_2, t)$ is determined by requiring that the membrane flow induced by this equation obeys local incompressibility. Thus, we must demand that the surface element does not change,

$$\partial_t \sqrt{g} = 0, \tag{41}$$

which implies explicitly

$$g^{ij} \mathbf{R}_i \partial_j (\partial_t \mathbf{R}) = 0. \tag{42}$$

Upon insertion into the equation of motion (40) with (35) and (32), the condition (42) becomes a partial differential equation for the unknown tension $\Sigma(s_1, s_2, t)$.

Equations (40) and (42) yield a deterministic evolution equation for a membrane configuration under the action of bending energy and hydrodynamics [48]. For any given initial membrane configuration, the solution to these equations will run into the next dynamically accessible local minimum of bending energy. In general, these equations must be solved numerically.

4.3   Equilibrium dynamics

For small perturbations around highly symmetric membrane configuration, the above scheme can be solved analytically. This allows the determination of relaxation times for thermal fluctuations in equilibrium. The simplest case is a planar membrane for which dynamical fluctuation can be calculated as follows. The time-dependent membrane configuration is written in Monge representation as

$$\mathbf{R}(x, y, t) = \begin{pmatrix} x \\ y \\ h(x, y, t) \end{pmatrix} \tag{43}$$

If an initial displacement $h(x, y, 0) = h_{\mathbf{q}}e^{i\mathbf{q}\mathbf{r}}$ with $\mathbf{r} = (x, y)$ is put into the equation of motion (40) with ($\mathbf{v}^{\mathrm{ex}} = 0$) one finds after some calculation a relaxation behaviour

$$h(x, y, t) = h(x, y, 0)e^{-\gamma_q t} \tag{44}$$

with $\gamma_q = \kappa q^3/\eta$, first derived in [44] slightly differently. According to the usual fluctuation-dissipation relation [19], the dynamical correlation functions follow as

$$< h_q(t)h_q^*(0) >=< |h_q|^2 > e^{-\gamma_q t}, \tag{45}$$

with $< |h_q|^2 >=< h_q(0)h_q^*(0) >$ given by (13). In a quasi-spherical geometry, a similar calculation using spherical harmonics yields relaxation rates $\gamma_{l,m}$ which can be compared to experiments, for some of the latest studies see [50, 51].

For non-spherical shapes, dynamical equilibrium fluctuations have been investigated for prolate shapes in the vicinity of the budding transition [52]. Another particularly interesting example of dynamical fluctuations has been observed at the prolate-oblate transition. Since the activation energy between the prolate and the oblate shapes is just a few $k_B T$, occasionally thermal fluctuations are large enough to drive the vesicle into the other minimum. This system thus constitutes one of the few examples showing a thermally induced macroscopic bistability [53].

4.4   Vesicle in shear flow

A vesicle in infinite shear flow was the first case for which the equation of motion derived in 4.2 was applied numerically [54]. An external shear flow with shear rate $\dot{\gamma}$ in x-direction

$$\mathbf{v}^{\mathrm{ex}}(\mathbf{r}) = \dot{\gamma}y\mathbf{e}_x = \dot{\gamma}[(y/2)\mathbf{e}_x + (x/2)\mathbf{e}_y)] - (\dot{\gamma}/2)\mathbf{e}_z \times \mathbf{r} \equiv \mathbf{v}^{\mathrm{el}}(\mathbf{r}) + \mathbf{v}^{\mathrm{rot}}(\mathbf{r}) \tag{46}$$

can be decomposed into an elongational component $\mathbf{v}^{\mathrm{el}}(\mathbf{r})$ which is tilted at $45°$ and a rotational component $\mathbf{v}^{\mathrm{rot}}(\mathbf{r})$, see Fig. 16.

Fig. 17 shows the result of the numerical implementation of the dynamical equations. An initial
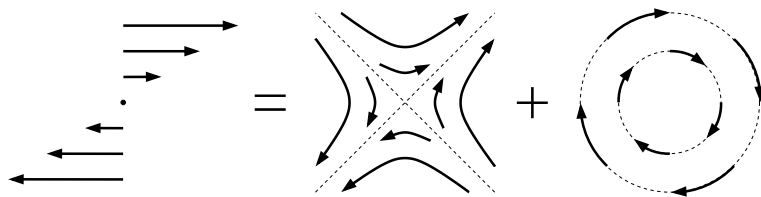
Fig. 16: *Decomposition of shear flow into an elongational and a rotational component.*
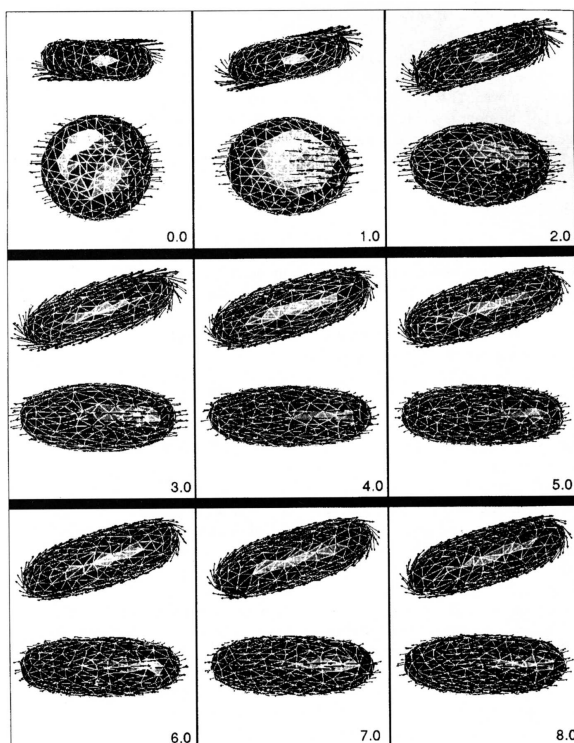

Fig. 17: *Evolution of an initially oblate vesicle under shear flow. The arrows denote the local velocity* [54].

equilibrium shape is at time $t = 0$ exposed to shear flow. The shape begins to elongate which immediately breaks the initial axi-symmetry. It tilts. After some time it acquires a stationary tilted elongated shape around which the membrane perpetually revolves in a so-called tank-treading motion. The qualitative features of this dynamically induced shape transformation can be understood on the basis of the decomposition (46). The elongational component leads to the tilt, whereas the rotational component leads to the tank-treading motion.

The quantitative analysis [54] shows that the tilt θ depends on the reduced volume (with $\theta \to \pi/4$) for $v \to 1$ as expected from the decomposition (46). The tilt is almost independent of shear rate $\dot{\gamma}$. This behaviour cannot persist to $\dot{\gamma} \to 0$ since one would expect to recover the equilibrium shape in this limit, which is however, difficult to reach numerically. The tank-treading frequency $\bar{\omega}$ (averaged over the shape) increases with reduced volume approaching $\dot{\gamma}/2$ for $v \to 1$ as expected.

Experimentally, a vesicle in shear flow has been studied in a slightly different regime [55]. The vesicle was initially spherical with thermal fluctuations. With increasing shear flow, some area stored in these fluctuations is "pulled out" and the shape elongates. With increasing shear rate

this elongation saturates since the total area is conserved. The tilt is initially $45°$ and becomes smaller with increasing shear rate. Since the algorithm described above does not include the effect of fluctuations (yet) a direct comparison is not possible. Analytically, however, one can include thermal fluctuation as long as one keeps the quasi-spherical approximation. Details of such a calculation using Langevin equations for the shape hydrodynamics [56] are given in [48].

4.5   Dynamically induced unbinding

For vesicles interacting with a substrate, shear flow can lead to a dynamically induced unbinding or detachment transition as observed in two recent experiments [57, 58], see Fig. 18. For small shear rate $\dot{\gamma}$, the vesicle tanktreads along the substrate. At a critical shear rate $\dot{\gamma}_c$, the vesicle starts to detach from the substrate.

A lift force occurs because of a symmetry breaking. The Stokes equation (31) are time-reversal invariant. This implies that a rigid sphere (or a tense vesicle) in shear flow at a certain height above a substrate will neither experience lift nor a force towards the substrate but rather translate at constant height. For a non-spherical shape, however, the fore-aft symmetry is broken and lift can occur.

If the vesicle is filled with a denser fluid than the environment, it hoovers at a distance h above the substrate. In such a stationary state the gravitational force will be compensated by the lift force. In the absence of a density difference between interior and exterior, the lift force leads the vesicle continuously further away from the substrate.
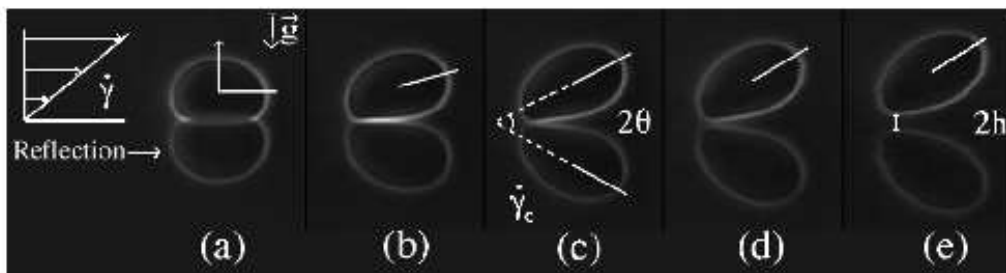
Fig. 18: *Experimental study of shear-flow induced unbinding of a vesicle from a substrate; (a): rest state; (b-d): vesicle elongates and tilts; (e): a gap develops between vesicle and substrate* [58].

Fig. 19: *Theoretical study of shear-flow induced unbinding in the same geometry* [59].

The theoretical work on this effect can be roughly classified as follows. The simpler two-dimensional problem (a semiflexible ring polymer above a one-dimensional line substrate) has been studied in [60]. A perturbative approach is possible at large separation $h \gg R$ for ellipsoidal shapes. It leads to a lift force $\sim \dot{\gamma}/h^2$ [61]. In three dimensions, a simple scaling

approach has given a rough picture of this unbinding transition in the regime of strong adhesion [62].

We now describe the results of a numerical study of the full three-dimensional problem [59]. Such a numerical analysis is possible only, since the Oseen-tensor for a half-space geometry is known exactly [63] as reproduced in footnote 22 of [59]. To retrieve the bare contribution of hydrodynamics to the lift force, adhesion and gravity were first turned off. The vesicle is initially at a small distance from the wall and then shear flow is imposed. In Fig. 19, a typical sequence of "snapshots" are shown. The initially oblate-like shape tilts, elongates, becomes prolate and finally takes off. The steady tilt of the vesicle plays the leading role in breaking the fore–aft symmetry of the vesicle with respect to shear flow. Since the tilt is almost independent of shear rate, the excess pressure in the space between the vesicle and the wall causes a lift force which is proportional to shear rate $\dot{\gamma}$. Additional effects due to the deformation are of $O(\dot{\gamma}^2)$. When gravity is included by implementing a density difference between the fluids inside and outside the vesicle, the vesicle indeed hovers at a constant distance from the substrate . Finally, for vesicles adhering to a substrate by the influence of a potential $V(l)$, a critical shear rate was found above which the vesicle unbinds from the wall. This critical shear rate is roughly linear in the adhesion strength w [59].

5   Perspectives

In the three main sections of this lecture, I described the analysis of the simplest model systems which show the phenomenon we wanted to understand, like the different shapes, adhesion and dynamics in hydrodynamic flow. By focusing on the simplest cases, the parameter space is small enough to allow for a comprehensive study. These studies prepared the ground for investigating more complex systems. Many applications or a more detailed modelling of biological systems require that some of the simplifying assumptions must be relaxed and further ramifications be introduced. These more complex models necessarily contain more parameters which makes a comprehensive study more difficult and often not even desirable. In this concluding section, I will mention a few such perspectives with some recent references. The interested reader will easily find more literature by searching the various data bases via the internet.

Vesicle membranes need not consist of only one sort of lipid. Lipid mixtures on curved shapes allow for a coupling between local composition and curvature as it has been shown recently in a beautiful experimental study [64]. Shape transformations induced by light or by changing the chemical composition are reviewed in [65]. Fusion of vesicles has recently been visualized using microfluoresence spectroscopy [66]. A quantitative modelling of such topological changes will require a more microscopic approach.

Adhesion needs not to be on a laterally homogeneous substrate as described here. Technologically interesting substrates may be chemically or morphologically structured as the one recently been used in the context of adhesion on silicon chips [67]. Adhesion can be counteracted by pulling with localized point forces which gives rise to force-induced detachment [68].

Dynamics is a huge field where we described the Oseen-tensor approach in some detail. A complimentary theoretical technique uses a phase field for studying vesicles in shear flow [69]. Other geometries like flow of vesicles in a cylinder or in a porous network are important for certain applications. Hydrodynamic flow also introduces long range interactions between two or several vesicles. For denser systems like vesicle suspensions, macroscopic rheological parameters should be determined on the basis of such mesoscopic studies.

One of the original motivations for studying vesicles as mentioned in the introduction was the quest for understanding the shapes and the elastic behaviour of red-blood cells. For a successful modelling, the polymeric spectrin network which endowes these cells with shear elasticity must be included. Shape transformations of these cells [70] and their fluctuations [71] have recently indeed been described by the interplay of the various elasticities of this compound membrane.

For other cells like leucocytes one wants to understand their adhesion to capillary walls in blood flow. Quite generally, biological adhesion is dominated by specific receptor/ligand molecules rather than by an unspecific adhesion due to physical interactions described here. How this specific interaction competes with hydrodynamically induced forces in cell detachment is a fascinating and open problem [72].

A general characteristics of cells is that they are genuine non-equilibrium systems. While we have discussed non-equilibrium aspects caused by hydrodynamic flow, important modifications also arise from the fact that in biological systems active processes happen which transform chemical energy into mechanical motion. The physics of such active membranes is reviewed in [73].

These few and necessarily pretty scattered remarks on some of the perspectives of the work described in this lecture demonstrate that vesicle research is not only a vivid topic in statistical physics. In retrospect in a couple of decades, this research may well be seen as having contributed first steps towards a quantitative understanding of cell biology. Within such a vision, the canon of physics, shaped in the twentieth century by fields like elementary particle physics, nuclear physics, atomic physics and solid state physics, will include not only soft matter physics, which is presently being established, but may even comprise a field ultimately called "cell physics".

Appendices

A   Differential geometry for vesicles

The membrane configuration $\mathbf{R}(s_1, s_2)$, parametrized by internal coordinates (s_1, s_2), is embedded in the three dimensional space. This space will be parametrized by Cartesian (x, y, z) or spherical (r, θ, ϕ) coordinates as $\mathbf{r} = x_\alpha \mathbf{e}_\alpha = r\mathbf{e}_r$ where $\alpha = x, y, z$. Summation over double indices is implied throughout the article. There are two tangential vectors

$$\mathbf{R}_i \equiv \partial_i \mathbf{R}(s_1, s_2) \quad \text{for} \quad i = s_1, s_2, \tag{47}$$

from which one obtains the metric tensor

$$g_{ij} \equiv \mathbf{R}_i \cdot \mathbf{R}_j. \tag{48}$$

Its determinant, $g \equiv \det(g_{ij})$, yields the area element

$$dA = \sqrt{g}\, ds_1 ds_2. \tag{49}$$

The normal vector, $\mathbf{n}(s_1, s_2)$, is given by

$$\mathbf{n} = \frac{\mathbf{R}_1 \times \mathbf{R}_2}{|\mathbf{R}_1 \times \mathbf{R}_2|}. \tag{50}$$

Finally, the mean and the Gaussian curvature follow from the curvature tensor

$$h_{ij} \equiv (\partial_i \partial_j \mathbf{R}) \cdot \mathbf{n} \tag{51}$$

as

$$H \equiv \frac{1}{2} \, h^i{}_i \tag{52}$$

and

$$K \equiv det(h^i{}_j), \tag{53}$$

where $h^i_j \equiv g^{ik} h_{kj}$ and g^{ij} are the matrix elements of the matrix inverse of (g_{ij}). Following the convention used in differential geometry, a sphere with the usual spherical coordinates $(s_1 = \theta, s_2 = \phi)$ has $H < 0$.

B   Steric of fluctuation potential

In this appendix, the derivation of the steric of fluctuation potential $V_{\mathrm{f}}(l)$ for a membrane under tension is sketched according to [30]. For a tensionless membrane, $V_{\mathrm{f}}(l)$ has been derived much earlier [35].

We consider a membrane pushed by a linear potential $+pl$ towards a rigid wall at $l = 0$. Its free energy functional becomes

$$F = \int dA \left\{ \frac{\kappa}{2} (\nabla^2 l)^2 + \frac{\Sigma}{2} (\nabla l)^2 + pl \right\} \simeq \int dA \left\{ \frac{\kappa}{2} (\nabla^2 l)^2 + \frac{\Sigma}{2} (\nabla l)^2 + pl + V_{\mathrm{f}}(l) \right\} \tag{54}$$

with configurations restricted to $l(\mathbf{r}) > 0$. For the second step, we have assumed that this geometrical constraint can be replaced by a smooth unknown repulsive potential $V_{\mathrm{f}}(l)$. Expanding around the minimum l_0 with $p = -V_{\mathrm{f}}'(l_0)$ and $h(\mathbf{r}) \equiv l(\mathbf{r}) - l_0$, we get after a Fourier transformation

$$F = \frac{1}{2} \int \frac{d^2 q}{(2\pi)^2} \left(\kappa q^4 + \Sigma q^2 + V_{\mathrm{f}}''(l) \right) |h_q|^2 \tag{55}$$

where we dropped the index 0 at l_0 again. On small length scales, $q > 1/\xi$, the harmonic energy (55) is dominated by the elastic part $\kappa q^4 + \Sigma q^2$; on large scales $q < 1/\xi$ the fluctuations feel the steric potential. The correlation length ξ can be defined precisely by

$$\kappa/\xi^4 + \Sigma/\xi^2 = V_{\mathrm{f}}''(l), \tag{56}$$

where ξ depends implicitly on l (the mean distance from the substrate), or l on ξ.

The confinement leads to a free energy density $f = b(kT)/\xi^2$. This form basically follows from a dimensional analysis, assuming that ξ is the only relevant length scale. The numerical prefactor b is of order 1. In the present context, f corresponds to $V_{\mathrm{f}}(l)$, which implies with (56) the non-linear differential equation

$$\kappa \left(\frac{V_{\mathrm{f}}(l)}{bkT} \right)^2 + \Sigma \left(\frac{V_{\mathrm{f}}(l)}{bkT} \right) = V_{\mathrm{f}}''(l) \tag{57}$$

for the fluctuation potential. The unique solution of this differential equation which diverges for

$l \to 0$ and vanishes for $l \to \infty$, is

$$V_f(\Sigma; l) = \left(\frac{6b^2(k_B T)^2}{\kappa l^2} \right) \left(\frac{y^2}{\sinh^2 y} \right) \quad \text{with} \quad y \equiv (\Sigma/bT)^{1/2} l/2, \tag{58}$$

given in eq. (19).

For tensionless membranes, where $\Sigma = 0$, the second bracket becomes unity. This form corresponds to the well-known Helfrich potential [35]. The numerical prefactor $6b^2 \simeq 0.1$ can be estimated by Monte-Carlo simulations [34]. In the presence of a lateral tension Σ, which pulls at the membrane, the power law decay of the first bracket is cut-off by the second factor at a length-scale $l_\Sigma \equiv (4bT/\Sigma)^{1/2}$ [34]. The best choice for b in this case is $b = 1/2\pi$.

C   The Oseen-tensor

In this appendix, we sketch the derivation of the Oseen-tensor according to [56]. The Stokes equations (31) read after Fourier transformation for all quantities with $e^{i\mathbf{k}\mathbf{r}}$

$$i\mathbf{k}p + \eta k^2 \mathbf{v} = \mathbf{f}$$
$$\mathbf{k}\mathbf{v} = 0 \tag{59}$$

Multiplying the first one with $-i\mathbf{k}$ and using the second leads to the pressure

$$p = -\frac{i\mathbf{k} : \mathbf{f}}{k^2} \tag{60}$$

being uniquely determined by the force. Here, : signifies the dyadic product $[(\mathbf{k} : \mathbf{f})_{\alpha\beta} = k_\alpha f_\beta]$. The first equation of (59) is now solved by

$$\mathbf{v} = \frac{1}{\eta k^2} \left(1 - \frac{\mathbf{k} : \mathbf{k}}{k^2} \right) \mathbf{f} \tag{61}$$

In real space, this relation becomes

$$\mathbf{v}(\mathbf{r}) = \int \mathcal{O}(\mathbf{r}, \mathbf{r}') f(\mathbf{r}') d^3 r' \tag{62}$$

with the Oseen-tensor

$$\mathcal{O}(\mathbf{r}, \mathbf{r}') \equiv \mathcal{O}(\rho) \equiv \frac{1}{\eta} \int \frac{d^3 k}{(2\pi)^3} \frac{1}{k^2} \left(1 - \frac{\mathbf{k} : \mathbf{k}}{k^2} \right) e^{-i\mathbf{k}\boldsymbol{\rho}} \tag{63}$$

Since the rhs is a tensor which depends only on $\rho \equiv |\boldsymbol{\rho}|$ with $\boldsymbol{\rho} \equiv \mathbf{r} - \mathbf{r}'$, its Cartesian matrix elements can be written as

$$\mathcal{O}_{\alpha\beta}(\rho) = A\delta_{\alpha\beta} + B\rho_\alpha \rho_\beta / \rho^2 \tag{64}$$

The scalars A and B are determined from the two equations

$$\mathcal{O}_{\alpha\alpha} = 3A + B \quad (\text{ summation over } \alpha \text{ understood }), \tag{65}$$
$$\mathcal{O}_{\alpha\beta}\rho_\alpha \rho_\beta / \rho^2 = A + B, \tag{66}$$

i. e.

$$3A + B = \frac{1}{(2\pi)^3} \int d^3k \frac{2}{\eta k^2} e^{-i\mathbf{k}\boldsymbol{\rho}} = \frac{1}{2\pi\eta\rho} \tag{67}$$

and

$$A + B = \frac{1}{(2\pi)^3} \int d^3k \frac{(1 - (\mathbf{k}\boldsymbol{\rho})^2/k^2\rho^2)e^{-i\mathbf{k}\boldsymbol{\rho}}}{\eta k^2} = \frac{1}{4\pi\eta\rho} \tag{68}$$

This leads to

$$A = B = \frac{1}{8\pi\eta\rho} \tag{69}$$

and hence the form (33) given in the main text.

References

[1] U. Seifert, Adv. Phys. **46**, 13 (1997).

[2] K. Berndl *et al.*, Europhys. Lett. **13**, 659 (1990).

[3] J. Käs and E. Sackmann, Biophys. J. **60**, 825 (1991).

[4] W. Wintz, H.-G. Döbereiner, and U. Seifert, Europhys. Lett. **33**, 403 (1996).

[5] X. Michalet and D. Bensimon, Science **269**, 666 (1995).

[6] X. Michalet and D. Bensimon, J. Phys. II France **5**, 263 (1995).

[7] P. B. Canham, J. Theoret. Biol. **26**, 61 (1970).

[8] W. Helfrich, Z. Naturforsch. **28c**, 693 (1973).

[9] U. Seifert, K. Berndl, and R. Lipowsky, Phys. Rev. A **44**, 1182 (1991).

[10] E. Evans, Biophys. J. **14**, 923 (1974).

[11] S. Svetina and B. Zeks, Eur. Biophys. J. **17**, 101 (1989).

[12] L. Miao, U. Seifert, M. Wortis, and H.-G. Döbereiner, Phys. Rev. E **49**, 5389 (1994).

[13] M. Jaric, U. Seifert, W. Wintz, and M. Wortis, Phys. Rev. E **52**, 6623 (1995).

[14] H. J. Deuling and W. Helfrich, J. Physique **37**, 1335 (1976).

[15] U. Seifert, Z. Phys. B **97**, 299 (1995).

[16] F. Jülicher, U. Seifert, and R. Lipowsky, J. Phys. II France **3**, 1681 (1993).

[17] F. Jülicher, U. Seifert, and R. Lipowsky, Phys. Rev. Lett. **71**, 452 (1993).

[18] H. Engelhardt, H. P. Duwe, and E. Sackmann, J. Physique Lett. **46**, L 395 (1985).

[19] F. Schwabl, *Statistische Mechanik* (Springer, Berlin Heidelberg, 2000).

[20] M. A. Peterson, H. Strey, and E. Sackmann, J. Phys. II France **2**, 1273 (1992).

[21] M. Wortis, M. Jaric, and U. Seifert, J. Mol. Liq. **71**, 195 (1997).

[22] V. Heinrich, F. Sevsek, S. Svetina, and B. Zeks, Phys. Rev. E **55**, 1809 (1997).

[23] W. Haeckl, U. Seifert, and E. Sackmann, J. Phys. II France **7**, 1141 (1997).

[24] P. Meleard, C. Gerbeaud, T. Pott, and L. Fernandez-Puente, Biophys. J. **72**, 2616 (1997).

[25] H.-G. Döbereiner *et al.*, Phys. Rev. Lett. **91**, 048301 (2003).

[26] A. Zilker, H. Engelhardt, and E. Sackmann, J. Physique **48**, 2139 (1987).

[27] J. O. Rädler, T. J. Feder, H. H. Strey, and E. Sackmann, Phys. Rev. E **51**, 4526 (1995).

[28] U. Seifert and R. Lipowsky, Phys. Rev. A **42**, 4768 (1990).

[29] R. Lipowsky and U. Seifert, Mol. Cryst. Liq. Cryst. **202**, 17 (1991).

[30] U. Seifert, Phys. Rev. Lett. **74**, 5060 (1995).

[31] R. M. Servuss and W. Helfrich, J. Phys. France **50**, 809 (1989).

[32] E. Evans and W. Rawicz, Phys. Rev. Lett. **64**, 2094 (1990).

[33] S. M. Bailey, S. Chiruvolu, J. N. Israelachvili, and J. A. N. Zasadzinski, Langmuir **6**, 1326 (1990).

[34] R. Lipowsky, in *Structure and dynamics of membranes - from cells to vesicles*, Vol. 1B of *Handbook of biological physics*, edited by R. Lipowsky and E. Sackmann (Elsevier, Amsterdam, 1995), pp. 521–602.

[35] W. Helfrich, Z. Naturforsch. **33a**, 305 (1978).

[36] U. Seifert, in *Giant vesicles*, edited by P. Luisi and P. Walde (J. Wiley and Sons, Europe, 1999), pp. 71–91.

[37] R. Lipowsky and S. Leibler, Phys. Rev. Lett. **56**, 2541 (1986).

[38] M. Mutz and W. Helfrich, Phys. Rev. Lett. **62**, 2881 (1989).

[39] W. Helfrich, in *Structure and dynamics of membranes - from cells to vesicles*, Vol. 1B of *Handbook of biological physics*, edited by R. Lipowsky and E. Sackmann (Elsevier, Amsterdam, 1995), pp. 691–722.

[40] M. Kraus, U. Seifert, and R. Lipowsky, Europhys. Lett. **32**, 431 (1995).

[41] H. G. Döbereiner *et al.*, Phys. Rev. E **55**, 4458 (1997).

[42] R. Bar-Ziv and E. Moses, Phys. Rev. Lett. **73**, 1392 (1994).

[43] J. Happel and H. Brenner, *Low Reynolds number hydrodynamics* (Noordhoff International Publishing, Leiden, 1973).

[44] F. Brochard and J. F. Lennon, J. Physique **36**, 1035 (1975).

[45] E. Evans, A. Yeung, R. Waugh, and J. Song, in *The Structure and Conformation of Amphiphilic Membranes*, Vol. 66 of *Springer Proceedings in Physics*, edited by R. Lipowsky, D. Richter, and K. Kremer (Springer, Berlin, 1992), pp. 148–153.

[46] U. Seifert and S. A. Langer, Europhys. Lett. **23**, 71 (1993).

[47] J. Prost, J.-B. Manneville, and R. Bruinsma, Eur. Phys. J. B **1**, 465 (1998).

[48] U. Seifert, Eur. Phys. J B. **8**, 405 (1999).

[49] Z. C. Ou–Yang and W. Helfrich, Phys. Rev. A **39**, 5280 (1989).

[50] L. Miao, M. A. Lomholt, and J. Kleis, Eur. Phys. J. **9**, 143 (2002).

[51] T. Pott and P. Meleard, Europhys. Lett. **59**,   87 (2002).

[52] H.-G. Döbereiner, E. Evans, U. Seifert, and M. Wortis, Phys. Rev. Lett. **75**, 3360 (1995).

[53] H.-G. Döbereiner and U. Seifert, Europhys. Lett. **36**, 325 (1996).

[54] M. Kraus, W. Wintz, U. Seifert, and R. Lipowsky, Phys. Rev. Lett. **77**, 3685 (1996).

[55] K. H. de Haas *et al.*, Phys. Rev. E **56**, 7132 (1997).

[56] M. Doi and S. F. Edwards, *The Theory of Polymer Dynamics* (Clarendon Press, Oxford, 1986).

[57] B. Lorz, R. Simson, J. Nardi, and E. Sackmann, Europhys. Lett. **51**,   468 (2000).

[58] M. Abkarian, C. Lartigue, and A. Viallat, Phys. Rev. Lett. **88**, 068103 (2002).

[59] S. Sukumaran and U. Seifert, Phys. Rev. E **64**, 011916/1 (2001).

[60] I. Cantat and C. Misbah, Phys. Rev. Lett. **83**,   880 (1999).

[61] P. Olla, J Phys. II France **7**,   1533 (1997).

[62] U. Seifert, Phys. Rev. Lett. **83**, 876 (1999).

[63] J. R. Blake, Proc. Camb. Phil. Soc. **70**, 303 (1971).

[64] T. Baumgart, S. Hess, and W. Webb, Nature **425**, 821 (2003).

[65] H.-G. Döbereiner, Current Opinion in colloid & interface science **5**, 256 (2000).

[66] G. Lei and R. MacDonald, Biophys. J. **85**, 1585 (2003).

[67] G. Zeck and P. Fromherz, Langmuir **19**, 1580 (2003).

[68] A.-S. Smith, E. Sackmann, and U. Seifert, Europhys. Lett. **64**, 281 (2003).

[69] T. Biben and C. Misbah, Phys. Rev. E **67**, 031908 (2003).

[70] H. Lim, M. Wortis, and R. Mukhopadhyay, Proc. Nat. Acad. Sci. **99**, 16766 (2003).

[71] N. Gov, A. Zilman, and S. Safran, Phys. Rev. Lett. **90**, 228101 (2003).

[72] S. K. Bathia, M. R. King, and D. A. Hammer, Biophys. J. **84**, 2671 (2003).

[73] S. Ramaswamy and M. Rao, C. R. Acad. Sci. **2**, 817 (2001).